Sulfurous Zeosils for Dehydra-Decyclization of Tetrahydrofuran to Renewable Butadiene

Raisa Carmen Andeme Ela[1,2], Jorge Barroso[5], Gaurav Kumar[1,2], Kaivalya Gawande[4], Manish Shetty[3], Xinyu Li[1], Wei Fan[4], Bess Vlaisavljevich[5*], Paul J. Dauenhauer[1,2]*

[1] Department of Chemical Engineering and Materials Science, University of Minnesota, 421 Washington Avenue SE, Minneapolis, Minnesota 55455, USA

[2] Center for Sustainable Polymers, University of Minnesota, 207 Pleasant Street, SE, Minneapolis, MN, 55455, USA

[3] Artie McFerrin Department of Chemical Engineering, Texas A&M University, 400 Bizzell Street, College Station, Texas 77843, USA

[4] Department of Chemical Engineering, University of Massachusetts Amherst, 686 North Pleasant Street, Amherst, Massachusetts 01003, USA

[5] Department of Chemistry, University of South Dakota, 414 E Clark St, Vermillion, SD, 57069

*Corresponding authors: hauer@umn.edu; bess.vlaisavljevich@usd.edu

Abstract. Renewable 1,3-butadiene (1,3-BD, C_4H_6) was synthesized from the tandem decyclization and dehydration of biomass-derived tetrahydrofuran (THF) on weak Brønsted acid zeolite catalysts. 1,3-BD is a highly solicited monomer for the synthesis of rubbers and elastomers. Selective conversion of THF to 1,3-BD was recently measured on phosphorus-modified siliceous zeolites (P-zeosils) at both high and low space velocities, albeit with low per-site catalytic activity. In this work, we combined kinetic analyses and QM/MM calculations to evaluate the interaction of THF with the various Brønsted acid sites (BAS) of Boron (B)-, Phosphorus (P)-, and Sulfur (S)-containing silicalite-1 catalysts toward a dehydra-decyclization pathway to form 1.3-BD. Detailed kinetic measurements revealed that all three catalysts exhibited high selectivity to 1,3-BD *ca.* 64-96% in the order of S-MFI > P-MFI > B-MFI at a given temperature (360 °C). Notably, the S-MFI maintained a selectivity > 90% for evaluated all process conditions. The computational results suggested that the nature of the Brønsted acid sites and the adsorption energetics (relative THF-acid site interaction energies) are distinct in each catalyst. Additionally, the protonation of THF can be improved with the addition of a water molecule acting as a proton shuttle, particularly in S-MFI. Overall, S-containing zeosils exhibited the ability to control reaction pathways and product distribution in dehydra-decyclization chemistry optimization within microporous zeolites, providing another alternative weak-acid catalytic material.

Introduction. The impermanence of fossil fuel reserves and the hazards associated with their extraction, processing, and utilization has galvanized industry and academia into exploring substitute renewable feedstocks to produce sustainable energy, commodity and specialty chemicals[1,2]. These globally desired chemicals include conjugated dienes, of which 1,3-butadiene (1,3-BD, C_4H_6) is the most significant[1]. 1,3-BD is primarily used to produce synthetic rubber employed in the production of car tires, clothing, and automotive parts.

The global production of 1,3-BD was approximately 12 Mt in 2015[2], while its global demand for the same year was about 10.5 metric Mt[1]. The oversupply of 1,3-BD has stimulated the development of innovative processes that deploy butadiene, such as the incorporation of functionalized monomers into styrene-butadiene rubber to improve the properties of car tires[1,3,4]. Nonetheless, at least 95% of 1,3-BD is presently generated as a byproduct of the steam cracking process employed to manufacture ethylene and other commodities.[2,5] In the steam cracking process, heavier feeds such as naphtha (accounts for 55% of global production) increase the yield of butadiene, contrary to lighter feeds such as ethane (accounts for 30% of global production), derived from natural and shale gas. Lighter feeds are increasing in demand leading to a decrease in the production of 1,3-BD and a corresponding increase in prices.[1,5–8] Additionally, the separation of 1,3-BD from the C4 stream remains costly due to the associated high energy requirements.[1] Furthermore, this process has a negative environmental impact due to significant greenhouse gas emissions[8].

1,3-BD is also produced commercially through the *Houdry Catadiene Process*, which is comprised of the catalytic dehydrogenation of *n*-butane, and *n*-butenes,[9,10], and from ethanol in some parts of the world, including China, Eastern Europe, South America, and India[1]. The ethanol and C4 diols routes for 1,3-BD synthesis are gaining global interest due to the increasing availability of industrial bio-derived ethanol and diol stock chemicals.[1] Presently, bioethanol is produced industrially from wheat, corn, and sugar cane (first-generation biomass source). Consequently, to cater to global demands there has been intense research effort to produce bioethanol and other platform chemicals from second-generation lignocellulosic and third-generation algal sources with high techno-economic viability.[1,11–13]

The production of 1,3-BD from ethanol requires lower capital cost, but the reaction yield in the temperature range 300-600 °C is significantly lower in comparison to the cracking process.[1] For instance, for a process using ethanol feed and a magnesia (59%)-chromic acid (2%)-silica gel (39%) catalyst at 400-425 °C , the selectivity to 1,3-BD was reported as 56% with an overall reaction yield of 38%.[14, 1] Improved ethanol to 1,3-BD thermochemical routes are being devised, including the one-step Lebedev process that operates between the temperature range of 400-450 °C, employing a metal oxide catalyst ($ZnO\text{-}Al_2O_3$),[7,15] and the two-step *Ostromislensky* process, which uses a tantalum-silica catalyst in the temperature range 325-350 °C yielding acetaldehyde as an intermediate product[15] and the catalytic dehydrogenation of butenes.[16]

The efficient production of 1,3-BD from biomass-derived cyclic ethers, such as THF, is another potential sustainable pathway to meet future 1,3-BD demand.[17,18] Biomass-derived furfural is a common product from biomass acid hydrolysis treatment, resulting particularly from xylose dehydration.[19] Bio-furfural has been the biomass-based feedstock considered in multiple research studies to produce biomass-derived tetrahydrofuran (THF) via catalytic decarbonylation and hydrogenation.[20,21] Similarly, the cyclo-dehydration of 1,4 butanediol over an acid-catalyst such as ZSM-5 may also generate THF.[22] Various routes to produce 1,3-BD from THF have been reported. These include work by Vecchini et *al.*,[22] where they produced 1,3-BD from 1,4- and 1,3-BDO via THF as an intermediate. The dehydra-decyclization of THF occurred on a sodium phosphate catalyst at 375 °C yielding 31% 1,3-BD.[18,23] Similarly, Reppe et *al.* devised a process which involved intermediate formation of gaseous THF dehydrated in the presence of water on a monoammonium orthophosphate catalyst, achieving 1,3-BD yields over 98% and THF conversions greater than 99%.[23–25]

Prior work by Abdelrahman *et al.* explored the selective synthesis of 1,3-BD from the dehydra-decyclization of gaseous THF on various commercial and prepared aluminum- and phosphorous-containing catalysts at varying process conditions.[18] Their results suggested that Brønsted acid sites (BAS) lead to C-

O bond scission and subsequent alkenol (primarily 2-buten-1-ol) dehydration to form 1,3-BD. Nonetheless, there was no direct correlation between BAS density measured for these low acidity catalysts and their selectivity toward 1,3-BD.[18] Notably, these results indicated the need for improved design of higher performing catalysts, particularly with higher per-site activity.[26,27] Additionally, the generation of 1,3-BD occurs in competition with two major side reactions: (1) decyclization of THF (rate-limiting reaction step) without further dehydration, rendering intermediate alkenol species: 3-butene-1-ol, 2-butene-1-ol (most favoring towards subsequent 1,3-BD formation, in the temperature range 220-270 °C) and 3-buten-2-ol, and (2) retro-Prins (RP) fragmentation of alkenols, surface alkoxides, and THF to generate propylene and formaldehyde.[17,18,28] Works by Kumar et *al.*,[26] Jain et *al.*,[29] and Ji et *al.*[27] concluded that the weakly acidic sites, which are chemically dynamic as a function of the extent of hydration and the catalyst confining space (pore structure) affect catalytic activity, stability, and selectivity to dienes.

In this study, we investigated the individual and combined effects of the reactor variables (temperature, weight hourly space velocity [WHSV, catalyst contact time], and water content in the feed) on the catalyst performance and stability to maximize THF conversion and 1,3-BD selectivity with increased catalytic activity. We considered phosphorus-containing (P)-MFI, which has shown high 1,3-BD selectivity, albeit at low space velocities and temperatures, boron (B)-MFI, reported to be selective towards larger conjugated dienes such as pentadiene,[30] and sulfur (S)-MFI, which to the best of the authors' knowledge has not yet been tested for this chemistry, as well as their sodium equivalents, to probe the effect of ions in the framework on this chemistry. Although the acid sites in aluminum-doped MFI structures are well-studied in the literature,[18] the acid sites in zeosils with boric, phosphoric, or sulfuric acid analogs have not been thoroughly characterized. Therefore, we conducted combined quantum mechanics and molecular mechanics (QM/MM) computational studies to identify the potential catalytic acid sites and assess how they interact with THF.

Materials and Methods. *Material synthesis and characterization.* Tetrahydrofuran (HPLC grade, Sigma Aldrich), Tetrapropyl ammonium bromide, TPABr (98%), Tetraethoxy silicate, (TEOS, 98%), and Tetrapopyl ammonium hydroxide, (TPAOH, 1.0 M) were purchased and used without further modification. To synthesize the silica (Si)-MFI, and sodium (Na) Si-MFI, sodium hydroxide, NaOH aqueous solution (1.0 M), deionized (DI) water, and fumed silica CAB-O-SIL M5 (Cabot Corp.) were used.

To make Si-MFI, 11.47 g of DI water was added to a 20 ml Teflon bottle; to this, a mixture of about 5.05 g 1.0 M TPAOH solution and 3.49 g TEOS was added. This was followed by hydrolysis at 80 ^{o}C using a preheated oil bath, and the solution was kept under stirring at 500 RPM using a magnetic stirrer. After 24 hours of hydrolysis treatment, this solution was transferred to an autoclave and kept in an oven at 443 K for 24 hours of crystallization. Then, the solid products were washed using centrifugation using DI water. Finally, the sample was calcined for 12 hours at 823 K at a ramping rate of 1 K/min. For B, P and S active site impregnation, targeting a theoretical ratio of Si/X = 27 (X= B, P, S), 0.72 wt % aqueous phosphoric acid solution (H_3PO_4), 0.44 wt % aqueous boric acid solution (H_3BO_3), and 0.69 wt % aqueous sulfuric acid solution (H_2SO_4) were used. About 3.35 mL of the acidic solution were mixed with 0.4 g of calcined MFI and stirred on a magnetic stirrer at 300 RPM for five minutes. Then, the solution was dried at 70 °C under the static conditions, while covered with the aluminum foil. The dried powder was ground and calcined at 600 °C for 30 minutes, with a 90-minute ramp to 600 °C under flowing air at 100 mL/min.

Particle morphology and size of MFI and Na MFI prior to and after B, P, or S impregnation was determined via Scanning Electron Microscopy (SEM). Powder XRD patterns were collected using a Rigaku SmartLab diffractometer. The diffractometer was equipped with Cu Kα radiation produced at 40 mA and 45 kV. The measuring step size was set at 0.026˚. Argon physisorption measurements were conducted with Quantachrome Autosorb iQ, at 87 K following outgassing at 573 K for six hours. Surface area was calculated using the BET method. Reactive gas chromatography methodology was used in measuring the BAS density using tert-amilamine (tAA) as a titrant, in accordance with existing procedures [31,32]. The XPS measurements were conducted using a PHI Versa Probe III XPS system (ULVAC-PHI) with mono-chromated Al K_α X-ray source (1486.6 eV), employing a base pressure of 2.8 x 10^{-8} Pa. To position the sample on the sample holder, a piece of double-sided sticking tape was employed. At all times, charge

neutralization was conducted before survey and high-resolution measurements. For survey measurements, an X-ray spot size of 0.20 x 0.20 mm^2 was selected, working at 45 W under 15 kV, 280 eV pass energy and 1.0 eV/step. High-resolution spectra were obtained with an X-ray spot size of 0.10 x 0.10 mm^2, at 25 W under 15 kV, 55 eV pass energy and 0.1 eV/step. Atomic calculations were conducted using Multipak software, and for high-resolution spectra, charge correction of C 1s peaks (allocated to C-C and C-H) were referenced at 285.0 eV. For curve fitting, a combination of Gaussian/Lorenzian functions were employed, with a minimum Gaussian percentage of 80%. FTIR spectra were collected using Thermofisher Nicolet iS 50 attached to a Harrick variable temperature ATR accessory, at room temperature, 70 ℃, and 120 ℃, with about 20-minute intervals to allow for effective temperature increment and sample heating. Spectral resolution 2 was employed, and 100 scans per spectra were collected.

Flow reactor experiments. Catalyst screening was conducted in a micro-flow reactor integrated within a Gas Chromatograph (**Figure S1**) with product elution via chromatography column (Agilent, HP-Plot Q, 30 m, 0.32mm ID, 20 μm film thickness), according to a previously reported procedure [33]. Briefly, ~ 30 mg of catalyst, pressed to about 2.0 tons of pressure for 25 minutes, and sieved into 106 – 250 μm aggregates, was inserted into a GC inlet liner and secured with deactivated quartz wool plugs (Restek 24324). This was inserted into the front inlet of the GC which has been conditioned to accommodate and serve as the heating jacket of the reactor. Prior to analysis the assembled reactor liner was calcined in situ under air (99.997 %, Minneapolis Oxygen) at a ramp rate of 3.0 K/min to 673 K for 5.0 h. Then, the reactor bed was cooled to reaction temperature and purged with helium (99.99 %, Matheson) for at least 30 minutes before inserting the reactant. Afterwards, using a syringe pump (74,905-04, Cole Parmer), vaporized THF was swept into the catalytic bed at about 60 sccm. Product quantification was done using a combination of flame ionization detector (FID) and a methanizer (quantitative carbon detector, QCD, POLYARC) [34]. Gaseous separation of molecules by gas chromatography included: THF, 1,3-butadiene, propene, butenes, and generally other compounds. The conversion of THF was calculated based on number of carbon mols (ν_n) according to Equation 1. The reaction rate was calculated according to Equation 2, where V denotes volume of feed, υ denotes the volumetric flow rate, and m, the mass of catalyst. The carbon balance was calculated on a carbon number basis, according to Equation 3. The site-time-yield (STY) was calculated according to Equation 4, where F_i denotes molar flow rate. Selectivity was calculated according to Equation 5.

$$\%\, Conversion = \frac{\nu_{THF,t=0} - \nu_{THF,t=t}}{\nu_{THF,t=t}} \times 100 \qquad (1)$$

$$Reaction\ rate = \frac{\nu_{THF,t=t} \times \upsilon}{V \times m \times BAS} \qquad (2)$$

$$Carbon\ balance = \frac{4\nu_{THF,t=t} + 3\nu_{propene,t=t} + 4\nu_{BD,t=t} + 4\nu_{butene,t=t}}{4\nu_{THF,t=0}} \qquad (3)$$

$$STY_i = \frac{F_i}{m \times BAS} \qquad (4)$$

$$Selectivity_i = \frac{Carbon\ Product_i}{Carbon\ THF_{converted}} \times 100 \qquad (5)$$

Computational Studies. The initial structure of the MFI framework was obtained from the Database of Zeolite Structures.[35] The subsequent model was built by following the multicentered spherical cutoff.[36–40] That is, all atoms within a sphere with a radius of 9 Å and centered at a T12 site were considered. The dangling atoms at the periphery were saturated with H atoms to comply with the tetra-coordination of Si atoms. The resulting system contains nearly 600 atoms, which is infeasible to analyze via density functional theory (DFT). Therefore, a combined QM/MM approach was used (*i.e.*, the ONIOM methodology) as implemented in Gaussian 16.[37–40] ONIOM can model large molecules by dividing the system into two or three layers treated at different levels of theory. Usually, the region where the reaction of interest takes

place is calculated using a more accurate method, such as DFT, while the outer layers, with a higher number of atoms, are calculated using semiempirical methods or classical force fields. In this study, the high layer was defined by the atoms within a 3.2 Å radius sphere from the T12 site, and it was computed with M06-2X/def2-SVP.[41] The outer layer contained the remaining external atoms. It was treated using the AM1 semiempirical method.[42] The procedure to build the starting structures with boric, phosphoric, and sulfuric acid was as follows: first, a Si-O bond is broken at a T12 site. Then, the acid dissociates one proton which binds to the exposed O atom, and the exposed Si atom binds with the remaining acid fragment. This acid absorption process is illustrated in **Scheme S1** for the case of sulfuric acid. Full optimizations were carried out at the M06-2X/def2-SVP level for the high layer and AM1 for the real layer. Relative energy differences of these structures were compared with the corresponding ones for systems that were relaxed with frozen atoms in the real layer. Since no significant variation was shown, harmonic vibrational frequencies were calculated to locate the corresponding transition states with the frozen atoms in the real region. All calculations were carried out using the Gaussian 16 software.[42]

Results and Discussion. The dehydra-decyclization of tetrahydrofuran to produce renewable 1,3-butadiene was evaluated on the Brønsted acid sites of B-MFI, P-MFI, and S-MFI in a packed bed flow reactor. The apparent kinetic rates and the product distribution at varying process conditions were measured by systematic screening, including temperature (200-370 °C), weight hourly space velocity (1.9-19.1 h^{-1}), and water content in the feed stream (0-10 %, v/v). Additionally, the time-on-stream performance was evaluated to identify the extent of catalyst deactivation. Since the decyclization of THF has been reported as the rate-limiting reaction step in aluminum-containing ZMS-5, the THF interaction and its proton affinity with each of the potentially active acidic sites in B-MFI, P-MFI, and S-MFI were further determined by QM/MM calculations. Consistent with **Scheme 1**, the major products detected in the reactor effluent when the reactor temperature was below 360 °C were 1,3-BD (from the dehydra-decyclization pathway), propene and butenes (resulting from the retro-Prins condensation pathway).

Reaction Chemistry. The thermodynamics of three reactions relevant to dehydra-decyclization of THF are depicted in **Figure S2**. Ring-opening of THF to 3-butene-1-ol is unfavorable at all considered temperatures (200-375 ºC). Retro-Prins condensation of THF to propene and formaldehyde is thermoneutral at 225 ºC and becomes favorable at higher temperatures. In contrast, dehydra-decyclization of THF to butadiene and water is overwhelmingly thermodynamically favorable at all considered temperatures, indicating that the reaction should proceed to butadiene at equilibrium. The thermochemical values were obtained from the NIST webbook database.[17,18] Additionally, the QM/MM calculations show that deprotonation of Brønsted acid sites (BAS) requires a higher activation energy without water (*vide infra*).

Tandem decyclization and dehydration of tetrahydrofuran (THF) over a hypothetical Sulfur-MFI BAS is depicted in **Scheme 1** to form butadiene (1,3-BD) in a sequence of six intermediates including an open site (1), adsorbed THF (s), ring-opened reactant (3), and product butadiene and water (6). The most likely mechanism on solid acid active sites has been proposed to occur via alkenol intermediate species, 2-buten-1-ol.[17] In parallel, two viable mechanisms, either directly from adsorbed THF (2) or the ring-opened species (3), can produce propene and formaldehyde via retro-Prins condensation.

Structural and physicochemical properties of catalysts. The ring-opening dehydration and retro-Prins reaction on weak-acid catalysts will depend on the acidity of the active sites and the surrounding catalyst environment; in this case, the chemical kinetics depend on the heteroatom bonding to the silica framework. Structural properties, precisely pertaining to MFI-modified zeolites (P-MFI, B-MFI, S-MFI and their sodium ion versions) control diffusion rates as well as catalytic performance.[43] The particle morphology, size, and crystallography collected with SEM and XRD can be found in the supplemental document (**Figures S3 – S6**). Additionally, BET surface areas and pore properties (**Table 1**, **Figure S7**), which agree with previous reports, show consistent features across all six catalysts, with a slight decrease in surface area for Na MFIs, perhaps due to Na^+ adsorbed on the surface or confined in pore spaces.[44] These results indicate that the weak-solid-acid active sites exist within the MFI framework and are accessible to reactants. These observations are consistent with the work reported by Li et *al.* [17].

While the strong acid site associated with aluminum incorporation into silica framework is well described, impregnation of all-silica zeosils of MFI structure with sulfuric acid, boric acid, or phosphoric

acid can result in numerous structures, not all of which will be catalytically active. As shown in **Scheme 2**, phosphoric acid can exist within zeolite pores, or it can progressively dehydrate to form Si-O-P bonds with the surface as well as P-O-P bonds with other molecules of phosphoric acid. Kumar et *al.* effectively estimated the BAS density of self-pillared pentasil (SPP) impregnated with phosphorus at an atomic concentration of Si/P = 27 (169 μmol g^{-1}) *via* the Hoffman Elimination of tert-amylamine.[31] Additionally, Jain et *al.* determined using ^{31}P-NMR that the active sites in P-SPP consist of a free hydroxyl group (not hydrogen bonded), bonded to a P-site, and also anchored to the siliceous framework.[29] Similar structures have also been observed with the impregnation of boric acid within siliceous MFI. Kumar et *al.* investigated the effect of micropore environments in boron-containing all-silica zeolites (i.e., B-MFI (Si/B = 38.3), B-MWW (Si/B = 13.2), B-BEA (Si/B = 23.8)) for the dehydra-decyclization of 2-methyltetrahydrofuran to pentadienes.[30] They found that the chemical structure of the active sites in these catalysts was distinct and thus resulted in different rate-normalized reaction rates at a given process condition.[30] Most importantly, they characterized their BAS density *via in-situ* pyridine titration, obtaining values (i.e., B-MFI, Si/B = 38.3, BAS density = 49.5 μmol g^{-1}) that represent the catalytically relevant acid sites.[26] Sulfuric acid containing siliceous MFI is also expected to exhibit a variety of structures with both the silica surface and other molecules of sulfuric acid, as shown in **Scheme 2**. Correspondingly, the small BAS density values measured for the B-MFI and S-MFI in this work, below 10 μmol g^{-1}, suggests that tert-amylamine could not titrate all catalytically relevant sites.

Active element concentration on B-MFI, P-MFI and S-MFI was assessed via Inductively Coupled Plasma Spectroscopy (ICP-OES), as the standard technique utilized in previous studies.[18,30] The absence of a quantitative correlation between the elemental concentration in the bulk and catalysts activity (**Table 1** and **Figure 1**) prompted further studies to elucidate the active element distribution across the zeolite. The same wet impregnation method was used to achieve a loading of Si/X = 27 (X = B, P, and S). X-ray photoelectron spectroscopy (XPS) was used to scan the elemental composition on the surface of the three main catalysts (**Table 1**, **Figures S8 – S10**), and the results showed that the amount of active element in the siliceous frameworks varied both on the surface and in the interior (bulk) of the catalysts (**Table 1**). This discrepancy in elemental distribution on the surface and in the interior of the catalysts provides insight into the chemical structure of the catalytically relevant active sites, that is, anchored to the framework with free hydroxyl groups. The elemental concentrations detected via XPS were closer to the targeted Si/X ratio for the B-MFI and the S-MFI (i.e., Si/X = 27). This could imply that most boron and sulfur groups are preferably anchored to the surface of the catalysts through the wet impregnation method, perhaps in the form of dimeric complexes that are not catalytically active. This observation is supported with NMR analyses (**Figures S11 and S12**), which indicated a single active chemical state for P-MFI,[29] and multiple chemical configurations for B-MFI, including dimeric complexes that would decrease the activity of the material.[45] These chemical peaks could explain the differences in BAS densities measured *via* the Hoffman Elimination of tert-amylamine. The BAS measured for P-MFI are consistent with literature values reported for wet impregnation of P-sites,[31] and the measured BAS densities of B-MFI and S-MFI were significantly lower than P-MFI. As mentioned earlier, Kumar et *al.* measured the BAS density of B-MFI *via in-situ* pyridine titration and obtained a low density (i.e., B-MFI, Si/B = 38.3, BAS density = 49.5 μmol g^{-1}) [26].

Effect of heteroatom identity on 1,3-Selectivity. The reaction rate and product distribution of THF dehydra-decyclization can be tuned on the BAS of the B-MFI, P-MFI, and S-MFI catalysts by varying the temperature (200-370 °C) and the weight hourly space velocity (1.9-19.1 h^{-1}). Under identical confining environments, the comparative performance of all six catalysts was evaluated at similar THF conversion values of 17.2 – 25.3 % (**Figure 1A**), and at identical process conditions; 360 °C, WHSV of 1.9 h^{-1}, and absence of water in feed stream (**Figure 1B**). Above 360 °C, 1,3-BD selectivity decreased, and the selectivity of larger compounds increased. At comparable conversion (**Figure 1A**) achieved by varying the temperature and WHSV values, the sulfur MFI catalysts exhibited the highest ratio of dehydra-decyclization rate to retro-Prins condensation rate, albeit possessing the lowest conversion values per mass of catalyst, statistically significantly different from phosphorus MFI and boron MFI. Moreover, the S-MFI had a uniquely high selectivity to 1,3-BD, a superior performance maintained throughout all the

experimental conditions explored in this work (**Figures 1B** [identical process conditions], **1C and 1D**), significantly exceeding the selectivity performance of P-MFI[18], as displayed in **Figure 1A**, 1,3-BD selectivity of ~ 91.4 ± 1.2 % for P-MFI, and ~ 96.1 ± 1.3 % for S-MFI. Both, P-MFI and Na P-MFI exhibited comparable selectivity to 1,3-BD and normalized STYs. However, the effect of sodium ions was evident between the boron MFI catalysts, where B-MFI and Na B-MFI had equivalent conversion values, but the selectivity to 1,3-BD of the Na B-MFI was inferior (~64% vs ~58.5%, respectively).

Effect of space velocity on product distribution. The activity of the catalysts and product distribution were studied by varying the temperature (200-370 °C) and the weight hourly space velocity (1.9-19.1 h^{-1}). Predictably, a decrease in the rate of THF consumption with decreasing catalyst contact times (**Figure 1C** and **1D**, Tables S1 – S4) was observed. These data are consistent with previous reports.[18,26] As THF conversion rate decreased with increasing WHSV, from 1.9 to 10.5, and lastly 19.1 h^{-1} (**Figures 1B – 1D**), the selectivity to 1,3-BD increased, most notable for S-MFI, where the selectivity to 1,3-BD exceeded 98.5 % at WHSV of 19.1 h^{-1}.These results support the idea that 1,3-BD is the primary product.

Effect of water in feed on catalyst activity and 1,3-BD selectivity by experiments and computation. The activity and the selectivity of the catalysts was assessed as function of the water content in the feed stream (0-10 %, v/v). The purpose of this was to investigate the potential role of *in-situ* steaming to decrease the formation of large compounds that lead to catalyst coking. Additionally, water was considered to determine if an optimal level of hydration could continually expose catalytically active sites.[29] These hypotheses were evaluated experimentally and computationally (**Figure 2**, **Table 2, and Table S6**). Water is a by-product in the desired chemistry to conjugated diene formation, and the effect of water on carbon formation and acid site density could occur even without co-fed steam. Moreover, biomass feedstocks frequently contain water, so it is important to evaluate the trade-off of utilizing aqueous feedstocks as opposed to pre-evaporation costs.[46]

The effect of water in the dehydra-decyclization of THF has been found to be statistically significant in experimental trials (**Figure 2** and **Figures S14–S17**). As shown in **Figure 2**, a considerable decrease in THF conversion was observed for the siliceous zeolites (P-MFI, B-MFI, and S-MFI. Alternatively, an increment on the activity value was observed for their sodium versions (Na P-MFI, Na B-MFI, and Na S-MFI). The effect of increased water partial pressures in the feed on selectivity to 1,3-BD was consistent for all catalysts; the selectivity to 1,3-BD increased as the concentration of water increased in the feed stream (**Figure 2** and **Table S1**). Particularly, for P-MFI, at 370 ℃ and 1.9 h-1, the conversion decreased from 50.2% to 36.3%, and the selectivity increased from 89.4% to 90.4%, at 0% and 5% (v/v) water in feed, respectively (**Table S1**). Additionally, at comparable conversion values of 6.9 ± 2.4 % (0 % water in feed, 250 ℃, and WHSV 10.5 h^{-1}) and 7.5 ± 1.7 % (5 % water in feed, 360 ℃, and WHSV 10.5 h^{-1}), the selectivity of the catalyst to 1,3-BD was 92.9 and 95.4 %, respectively. These results, taken together, suggest that water precludes C-C bond fragmentation and suppresses competing side reactions and complex condensation reactions. Thus, the concentration of water in the reactor feed can be tuned to manipulate the selectivity to 1,3-BD.

It was observed via computation that water plays a crucial role in the selectivity to 1,3-BD. The bond distance between the proton and its oxygen increases if a water molecule is present (**Tables 2 and Table S6**). This suggests a weakening of the bond and, in turn, a lower energy is required to deprotonate. For both B-MFI and S-MFI, this O-H elongation is most pronounced at H2, 0.015 Å and 0.093 Å, respectively. In P-MFI, a bond elongation is generally observed with the exception of coordinating to the H1 site. There is a clear difference between the favored site for interaction among the three systems. In B-MFI and S-MFI, THF tends to interact more with the acidic groups, but in P-MFI it has a stronger interaction with the BAS on the surface of the framework. That is, in P-MFI, deprotonation is favored on H2 under dry conditions, but on Hzeo when water is included. Regarding deprotonation, the calculations show a significant preference for S-MFI in which 28.0 kcal/mol is required for the direct proton transfer of THF, while only 16.0 kcal/mol is required if the transfer is facilitated by the presence of water. That is, the acidic proton is shuttled by the water molecule, forming the hydronium ion, and from there to THF (**Figure 6**). In other words, the calculations corroborate the high potential of the sulfur-containing zeolite for obtaining 1,3-BD from THF. Further studies must be conducted to gain a better understanding of the dehydra-

decyclization mechanism and competing pathways to identify the specific variables leading to a higher THF conversion rate.

The role of water for increasing the selectivity to butadiene could result from, firstly, a decrease in the activity of the catalyst which in turn hinders competing chemistries. Secondly, calculations revealed that the barrier for proton transfer from the acid site to THF is lowered in the presence of water (**Table 2** and **Table S6**), and plausibly, the water in the system also decreases the desorption energy barrier of 1,3-BD, thus precluding the formation of undesired larger compounds, which could result from the oligomerization of formed 1,3-BD (**Table S7**).[47] The work by Jain et *al.* suggests that there is an active site chemical evolution for P-zeosils with continuous hydration, as proposed in **Scheme 2**. The computational results suggest water could enhance the reaction rate. Specifically, water would initially hydrolyze (X = P/B/S)-O-Si linkages, giving rise to X-OH linkages that increase BAS density.[29] Thus, theoretically, steaming could assist in exposing additional active sites from the B, P, and S dimeric complexes.

Overall catalytic performance. For all conditions explored in this work, a steady decrease in 1,3-BD selectivity was observed with increased catalytic activity (**Figure 4**). The highest performing catalyst with respect to 1,3-BD selectivity was S-MFI; its selectivity to 1,3-BD was initially above 96% for THF conversion below 10% and decreased to ~ 83% at THF conversion of ~ 36%. Increased conversion was attained by reducing the WHSV. P-MFI, B-MFI, and their Na^+ versions exhibited trends similar to S-MFI. Amongst all the catalysts tested in this study, B-MFI was the least selective towards 1,3-BD formation. Despite this, the selectivity can be increased from 68 ±1.3 to ~ 71.5 ± 1.5 % at a WHSV of 10.5 h^{-1} by co-feeding water (10 % v/v) to the reactor (**Figure 2**). Overall, P-MFI was the second-most selective catalyst with the highest THF conversion (given its significantly higher BAS concentration), and the highest yield, thus making it the most efficient catalyst overall.

P-MFI selectivity to 1,3-BD. We studied the activity and the selectivity of the catalysts by varying the temperature (200-370 °C), and the weight hourly space velocity (1.9-19.1 h^{-1}). An increased rate of conversion with temperature was observed experimentally with P-MFI catalysts at WHSV of 1.9 and 10.5 h^{-1} (**Figure S13 and Table S1**). We observed that the rate of THF conversion increased as the temperature increased, from 5.8 ± 3.5 % at 200 ℃ to 50.2 ± 1.4 % at 370 ℃, as expected. Similarly, for WHSV of 10.5 h^{-1} the conversion moderately increased from 4.9 ± 0.6 % at 200 ℃ to 16.7 ± 1.7 % at 370 ℃. Simultaneously, the selectivity to propene also increased, from ~ 0.95% to 5.2 % at WHSV of 1.9 h^{-1}, and ~ 1.0% to 3.2 % at WHSV of 10.5 h^{-1}. Conversely, the initially high selectivity to 1,3-BD decreased slightly as the temperature increased, by about 5.6 % and 3.6 %, at 1.9 h^{-1} and 10.5 h^{-1}, respectively (**Figure S13**). Over P-MFI within the temperature range explored (200 – 370 ℃), the selectivity to larger compounds increased by about 2.8 % at 1.9 h^{-1} (**Figure S13, Table S1**). A decrease in selectivity to butadiene could be due to 1,3-BD condensing into a larger molecule, commensurate with an increase in selectivity for larger compounds (**Figure S13**). Our results are consistent with the observations made by Ji et *al.* [27] which suggest that formed 1,3-BD can undergo oligomerization and reduce the overall selectivity toward 1,3-BD. These larger compounds could further react to coke and contribute to catalyst deactivation.

Apparent kinetics for tandem decyclization and dehydration of THF. Measured apparent kinetics for THF tandem dehydra-decyclization are presented in **Figure 4A** for a temperature range (200 – 400 ℃). Kinetics were measured at THF conversion limited to <18 % in accordance with previous procedures.[18] The apparent activation barriers to dehydra-decyclization (typed in **Figure 4A**) for all catalysts were similar. Particularly, the apparent dehydra-decyclization activation energy of P-MFI was determined as 24.1 ± 1.1 kcal/mol; similar values have been reported for this chemistry using P-SPP as a catalyst.[18] The apparent activation energies for S-MFI and B-MFI were measured as 26.6 ± 0.6 kcal/mol and 27.1 ± 1.7 kcal/mol, respectively. The apparent activation energies of these materials are the same within experimental error, suggesting that the catalytic mechanism is the same. Remarkably, S-MFI displayed the highest per site 1,3-BD formation rates (**Figure 4A**), and highest ratio of dehydra-decyclization rate to retro-Prins condensation rate across the entire temperature range, with per-site rates ~ 16 times greater than P-MFI at 360 ℃ and 1.9 h^{-1}. Thus, we conclude that for similar Si/X element loadings, the chemical coordination of the active sites and defects in the framework/support is crucial in determining catalytic performance.

The ratio of apparent rate of THF tandem decyclization and dehydration to form 1,3-BD (DH in **Figure 4B**) to apparent rate of THF and alkenol fragmentation via retro-Prins condensation to form propene (RP in Figure 4B) was highest for S-MFI, ~ 2x greater than P-MFI, and ~ 8x greater than B-MFI at the highest points (**Figure 4B**). The ratio of rate of dehydra-decyclization to rate of retro-Prins condensation (**Figure 4B**) does not account for other side products, which increase as the rate of PR increases. Overall, these results demonstrate the superior 1,3-BD selectivity and per-site THF conversion performance of S-MFI. The same trend was observed at a higher WHSV of 10.5 h^{-1}, confirming the maintained high selectivity at high and low conversion.

Deactivation of B-MFI, P-MFI, and S-MFI. The performance of the B-MFI, P-MFI, and S-MFI catalysts was evaluated under continuous THF feeding (time-on-stream analysis) at 360 °C, and 1.9 h^{-1} to study deactivation (**Figure 5**). Our results demonstrate that P-MFI active sites are more stable than the active sites in B-MFI and S-MFI, as the rate of THF conversion value and the selectivity of 1,3-BD fluctuated around the average value for a period of six hours. The THF conversion of B-MFI and S-MFI remained constant on average for about 5 and 4 hours, respectively. Then, their conversion values decreased by 26% and 53%, respectively. For S-MFI, when water was added to the feed at a concentration of 10 % (v/v), the initial conversion decreased as expected. The catalyst activity then stabilized, and minimal further deactivation was observed. For the specific slow deactivation of P-MFI, it is known that the micropores in MFI contribute to suppressing coke-promoted catalyst deactivation.[50] Additionally, work by Epelde et *al.* highlights that phosphoric acid (H_3PO_4) modified MFI suppressed the formation of coking molecules.[51] This could explain the higher stability of the P-MFI under reaction conditions.

Computational analysis. The coordination of H_3BO_3, H_3PO_4, or H_2SO_4 into the zeolite takes place by cleaving one Si-O bond at a T12 site (**Scheme S1**). A deprotonated O on the acid binds to the Si atom and the proton coordinates to the adjacent surface O atom, forming a BAS. Note that two acidic protons (H1 and H2) remain on B-MFI and P-MFI, and one on S-MFI (H1), which can then act as acid sites to protonate THF, in addition to the zeolite BAS (Hzeo). Since this step is crucial in the conversion of THF, the energetics for the different acidic sites were estimated. The bond lengths between the oxygen and the proton adsorbed on the surface (Hzeo) and with the protons attached to the acid moiety (H1 and H2) are reported (**Table S6**). In the case of B-MFI and P-MFI where there are two available protons, H1 is defined as the closest to Hzeo. In addition, the electron affinity (ΔE_{EA}) and interaction energy (ΔE_{IE} between each proton and an explicit water molecule are listed (**Table 2**). As expected, the longer O-H distances correspond to a proton from the acid fragment (H1 or H2), suggesting a higher ease of detachment by the water molecule. Specifically, for S-MFI, the detachment of H1 involves 1.9 kcal/mol less than for the proton on the surface (Hzeo). Also, its interaction with water and THF is 10.5 kcal/mol lower than with the latter (i.e., only in the case of S-MFI); both the interaction energy and the proton affinity are more favorable on H1.

Conclusions. A combination of packed bed flow reactor experiments, spectroscopic analyses, and QM/MM calculations was employed to study the gas-phase dehydra-decyclization of tetrahydrofuran on the weak Brønsted acid sites of boron-MFI, phosphorus-MFI, and sulfur-MFI as alternative sustainable routes for the efficient production of renewable 1,3-butadiene from lignocellulosic biomass. Kinetic measurements revealed that all three catalysts exhibit competitive selectivity to 1,3-butadiene *ca.* 50-99% in the order of sulfur-MFI > phosphorus-MFI > boron-MFI at both low (0%) and high (10%) water content in the feed stream for conversions $\geq$ 4%. Notably, the sulfur-MFI displayed the highest ratio of dehydra-decyclization rate to retro-Prins condensation rate, and maintained a selectivity toward 1,3-butadiene > 90% for all process conditions evaluated. Furthermore, the 1,3-BD formation rates could be increased by co-feeding water to the reactor, albeit at decreased tetrahydrofuran consumption rates. The QM/MM calculations revealed the formation of two acidic protons in the Boron-MFI and the Phosphorus-MFI, and one in the Sulfur-MFI, in addition to the zeolitic Brønsted acid site. Particularly, in the B-MFI and the S-MFI, tetrahydrofuran preferentially interacts with the additional acidic groups, and in the P-MFI its interaction is strongest with the zeolitic Brønsted acid site. Furthermore, Phosphorus-MFI deprotonation was found to be more favorable on one of the additional acidic sites under dry conditions, and more

favorable on the Brønsted acid site when water was included. This suggests that the additional acidic protons could contribute to the overall reaction chemistry. Additionally, the computational calculations suggest that the deprotonation energy barrier is lowest for the Sulfur-MFI, in accordance with the highest selectivity toward 1,3-BD measured experimentally.

Associated Content

Supplemental Information

The Supporting Information is available free of charge on the ACS Publications website at DOI:

> Schematic of reactor system. Vapor-phase thermochemistry plot. SEM micrographs of original silicious and sodium catalysts. XRD plots for original and impregnated catalysts. Ar physisorption isotherms. XPS analyses of P-MFI, B-MFI, and S-MFI. Summarized raw kinetics data for P-MFI, Na P-MFI, B-MFI and S-MFI. Summary charts of Tukey's and Box-Behnken analyses. Relative interaction energies of THF with acid sites. Relative energies of the dehydra-decyclization of THF. FTIR spectra of P-MFI, B-MFI, S-MFI and THF doped S-MFI as a function of temperature.

Author information

Corresponding Author

*E-mail: hauer@umn.edu

ORCID ID

Raisa C. A. Ela: 0000-0002-2096-4582
Jorge Barroso: 0000-0002-9715-8693
Gaurav Kumar: 0000-0001-7089-6146
Kaivalya Gawande: 0009-0000-2354-3874
Manish Shetty: 0000-0002-8611-7415
Xinyu Li: 0000-0001-9061-066X
Wei Fan: 0000-0002-8581-2651
Bess Vlaisavljevich: 0000-0001-6065-0732
Paul J. Dauenhauer: 0000-0001-5810-1953

Author Contributions

All authors contributed equally to this work.

Notes. The authors declare no competing financial interest.

Keywords. Biomass, Tetrahydrofuran, Butadiene, Decyclization, Dehydration, Silicalite-1.

Acknowledgements. The authors acknowledge the National Science Foundation (NSF), Center for Sustainable Polymers, Grant CHE-1901635, and the Characterization Facility of the University of Minnesota which receives support from NSF MRSEC. Part of Figure S1 was created in BioRender.com. The table of contents image was created with funds from the Mistletoe Research Fellowship (Momental Foundation). Computations supporting this project were performed on high-performance computing systems at the University of South Dakota, funded by NSF award OAC-1626516. BV and JB acknowledge that the land their research was performed on is the original homelands of the Dakota, Lakota, and Nakota tribal nations.

Table 1. Surface and physicochemical properties of all MFI catalysts.

Catalyst	Si/X by ICP[a]	Si/X by XPS[b]	BET Surface area ($m^2 g^{-1}$)	Micropore width (Å)	BAS ($\mu mol\ g^{-1}$)[c]	R_{SEM} (μm)[d]
B-MFI	71.5:1	15.1:1	447.8	6.8	9.1	0.39 ± 0.03
P-MFI	24.1:1	12.1:1	415.2	7.2	186.6	0.39 ± 0.03
S-MFI	46.7:1	22.1:1	446.1	7.2	5.5	0.39 ± 0.03
Na B-MFI	88.4:1	-	407.3	6.8	6.9	4.04 ± 0.33
Na P-MFI	24.8:1	-	431.5	7.2	96.6	4.04 ± 0.33
Na S-MFI	42.5:1	-	407.3	6.8	3.5	4.04 ± 0.33

[a] Values computed via ICP-OES.
[b] Values computed with X-ray photoelectron spectroscopy (XPS).
[c] Values determined by tert-amylamine Hoffman elimination.
[d] Particle radius calculated from at least 20 crystallites using SEM micrographs

Table 2. Distance (*r*) in Å of the O atom and the acid site (H1, H2, or Hzeo). Relative interaction energies (ΔE_{IE}) of THF with an explicit water molecule at acid sites. THF proton affinity energies (ΔE_{PA}). The deprotonation was computed by including one explicit water molecule. The H1 site corresponds to the acidic proton closest to the surface proton, Hzeo. Energies are in kcal/mol and computed at the M06-2X/def2-SVP:AM1 level.

	H1			H2			Hzeo		
	r	ΔE_{IE}	ΔE_{PA}	*r*	ΔE_{IE}	ΔE_{PA}	*r*	ΔE_{IE}	ΔE_{PA}
B-MFI	0.992	0.0	43.8	0.988	9.8	32.1	0.983	9.9	44.0
P-MFI	1.004	0.0	36.3	1.037	-5.1	34.4	1.006	-12.7	45.0
S-MFI	1.079	0.0	16.0	NA	NA	NA	0.971	10.5	17.9

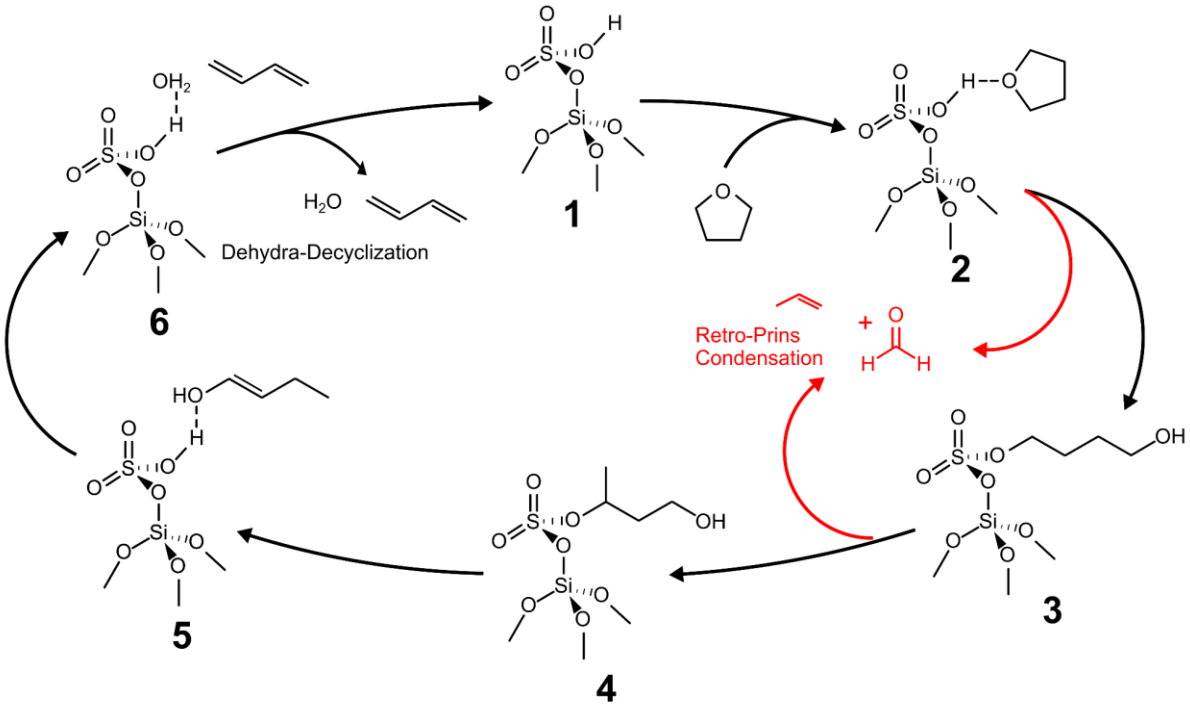

Scheme 1. Chemical reaction pathways and transformations of THF over Brønsted acid sites.

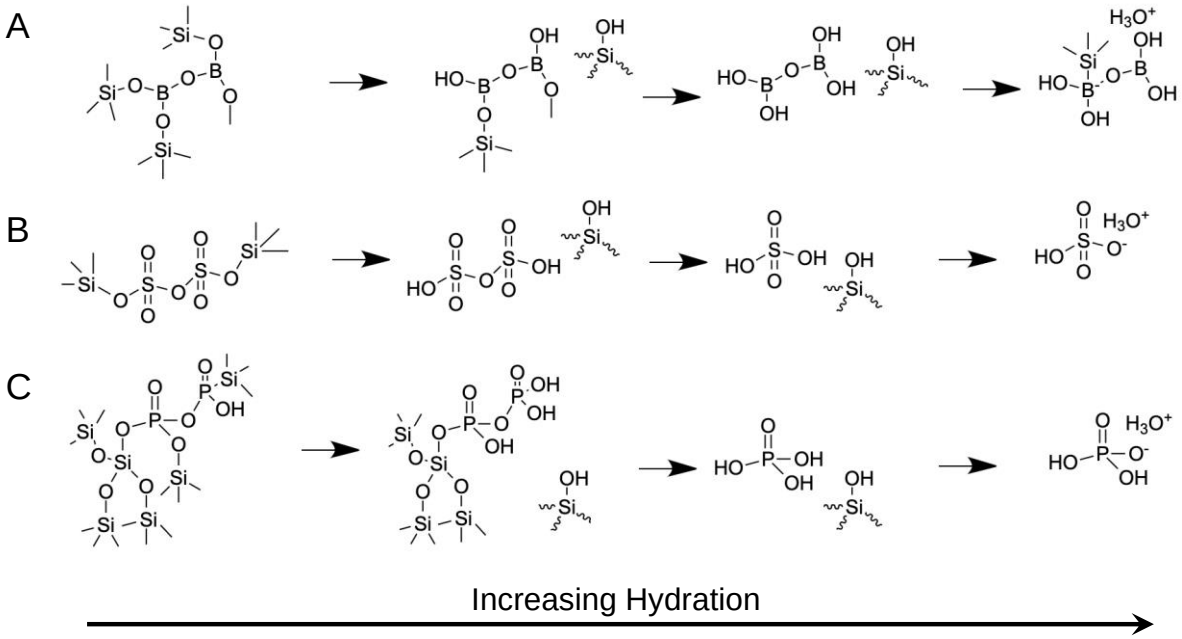

Scheme 2. Known active site evolution chemistries for P-MFI and B-MFI[29,30] and proposed pathway for S-MFI under continuous hydration.

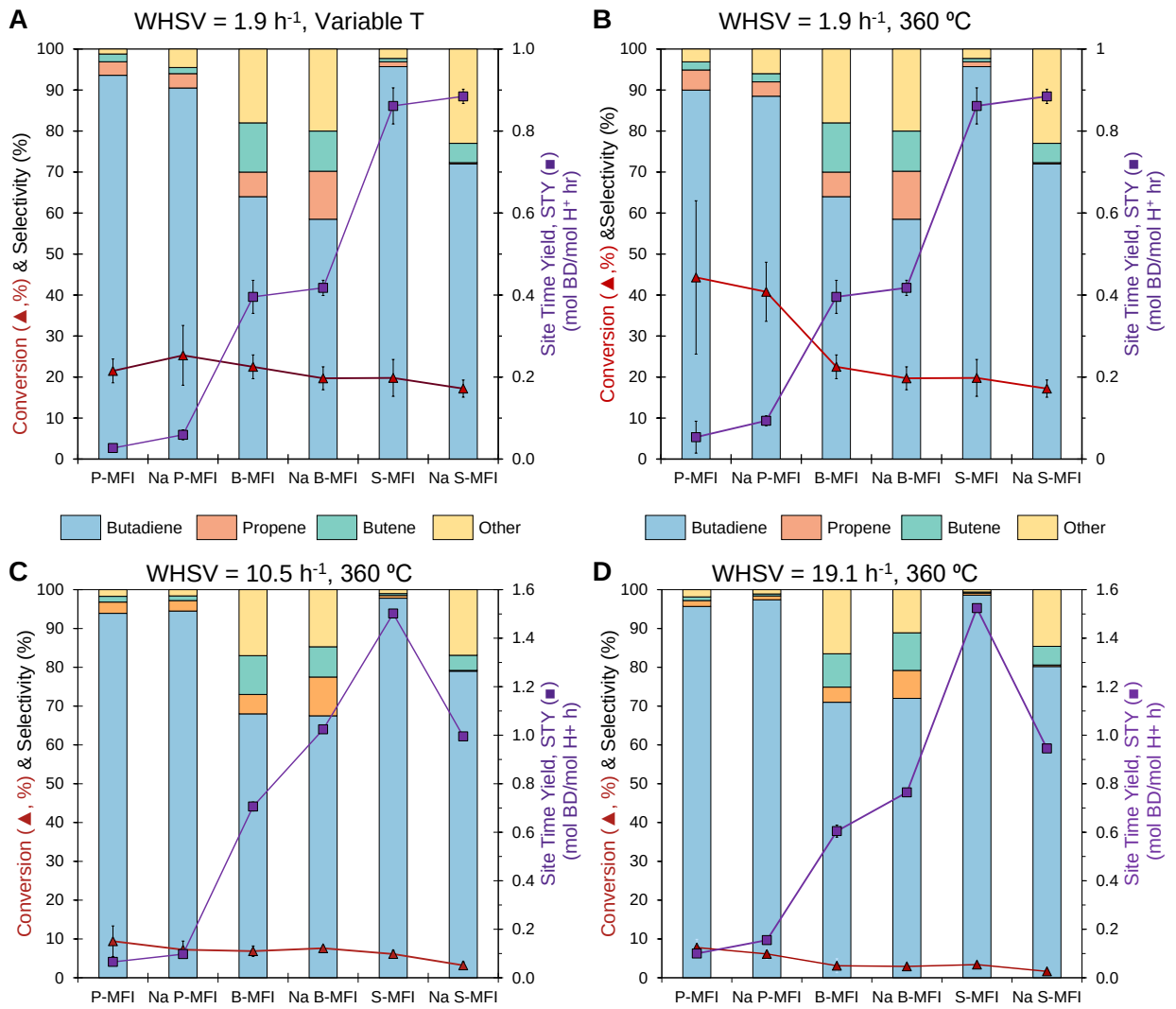

Figure 1. Dehydra-decyclization of THF with Weak Solid Acids. Six variations of weak solid acid catalysts were evaluated in a packed bed flow reactor to determine the rate of reaction (site time yield) and selectivity to products of butadiene (blue), propene (orange), butene (teal), and others (yellow). (A) Catalysts were evaluated at identical conversion (~26%), at a THF partial pressure of 3.7 torr, weight hourly space velocity of 1.9 h^{-1} and varying temperature (200 - 360 ºC). (B) Catalysts were evaluated at a THF partial pressure of 3.7 torr, identical temperature (360 ºC) and space velocity (1.9 h^{-1}) with varying conversion. (C) Catalysts were evaluated at a THF partial pressure of 20.1 torr, identical temperature (360 ºC) and space velocity (10.5 h^{-1}), (D) Catalysts were evaluated at a THF partial pressure of 35.8 torr, identical temperature (360 ºC) and space velocity (19.1 h^{-1}). Error bars represent the standard deviation computed for experimental runs (n) ≥ 3.

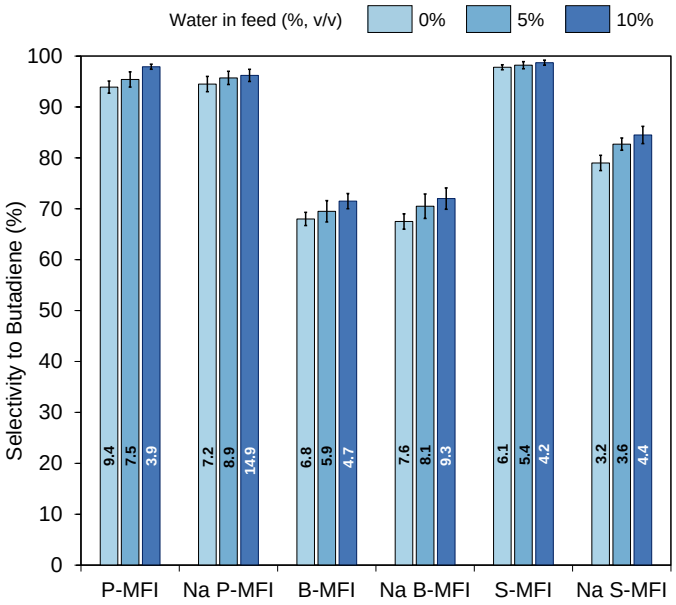

Figure 2. Catalytic selectivity to 1,3-BD of all six catalysts as a function of water content in feed stream at a THF partial pressure of 20.1 torr, 360 ℃ and feed WHSV of 10 h^{-1}. Different shades of blue bars represent 0%, 5%, and 10% of the feed THF containing water by volume. Error bars represent the standard deviation computed for experimental trials (n) $\geq$ 3. The numbers within bars stands for the conversion value.

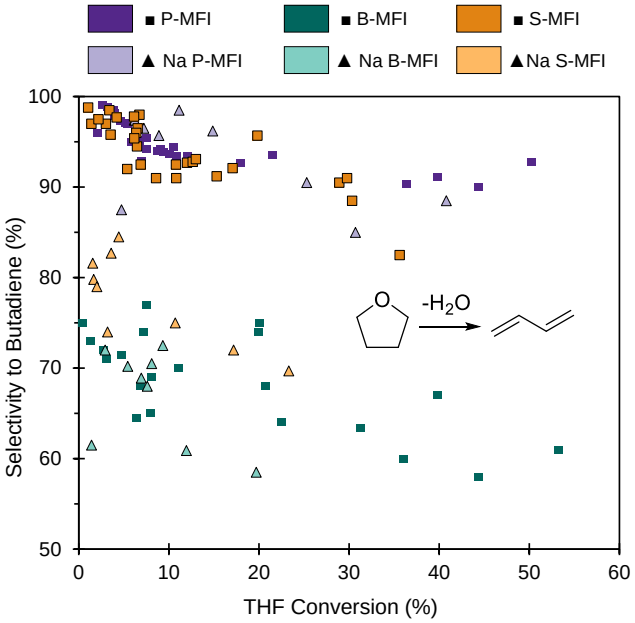

Figure 3. Dehydra-decyclization of THF to butadiene at variable conditions: 200-360 °C, THF partial pressures of 1.1 – 35.8 torr, WHSV of 0.5–19.1 h^{-1}, and 0–10 vol% water in feed stream. Additional details in supporting information.

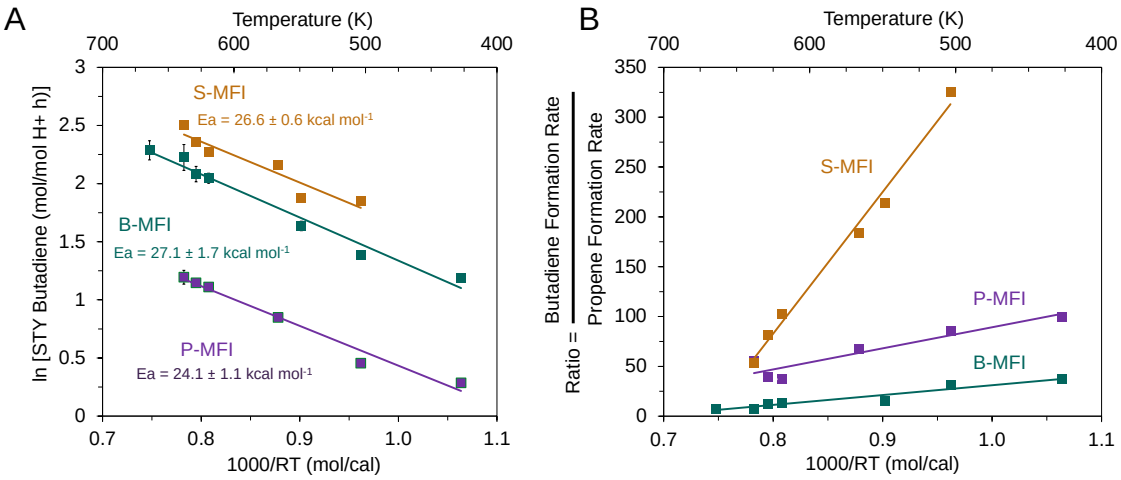

Figure 4. (A) Arrhenius plots for apparent 1,3-BD formation rates for P-, B-, and S-MFI at 1.9 h^{-1} and 0 % water in feed. Apparent activation energies are measured at THF partial pressure 3.7 torr, WHSV 1.9 h^{-1} for THF conversions < 18 %. Dashed lines in **A** are linear fits to the data points. **(B)** Temperature effect on ratio of apparent rate of tetrahydrofuran (THF) dehydra-decyclization to form 1,3-butadiene (BD) via dehydration (DH) to apparent rate of THF fragmentation via retro-Prins to form propene (RP) for P-, B-, and S-MFI at THF partial pressure 3.7 torr, WHSV 1.9 h^{-1} and 0 % water in feed. Error bars represent the standard deviation computed for experimental runs (n) ≥ 3.

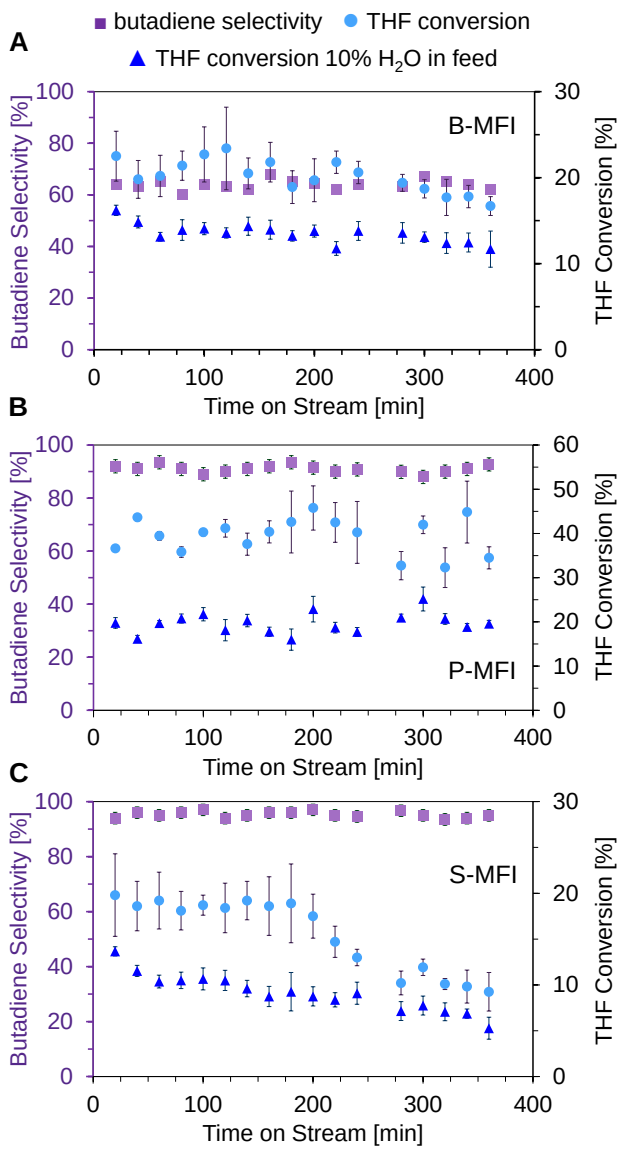

Figure 5. Conversion of tetrahydrofuran (THF) and selectivity to 1,3-butadiene as a function of time on stream at THF partial pressure 3.7 torr, WHSV 1.9 h^{-1}, 360 °C, for 0 % and 10 % v/v water in feed stream for six hours. Error bars represent the standard deviation computed for experimental trials (n) ≥ 3 over catalysts **(A)** B-MFI, **(B)** P-MFI, and **(C)** S-MFI.

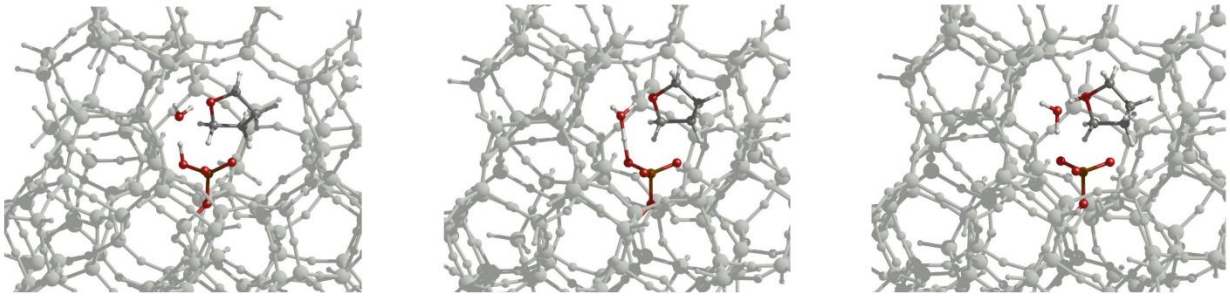

Figure 6. Tetrahydrofuran protonation steps from intermediate INT-I to intermediate INT-II through transition state TS_{I-II} involving an explicit water molecule. Energies in kcal/mol computed at the M06-2X/def2-SVP:AM1 level.

Table of Contents Image

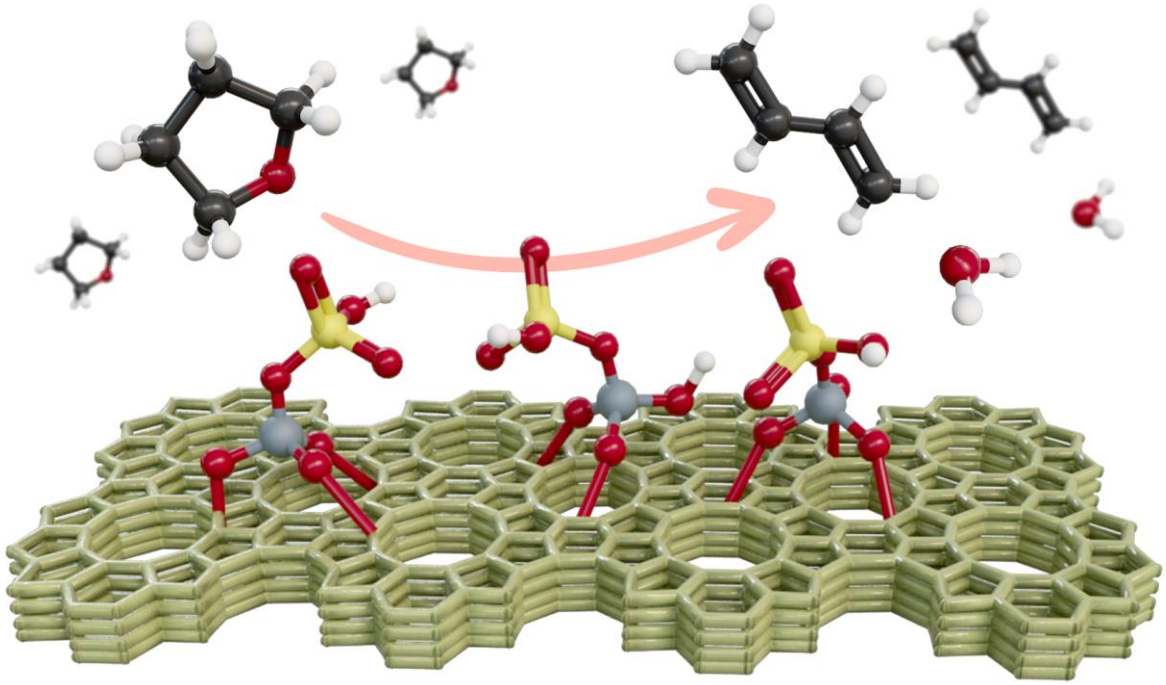

References

1. Makshina, E. V. *et al.* Review of old chemistry and new catalytic advances in the on-purpose synthesis of butadiene. *Chem. Soc. Rev.* **43**, 7917–7953 (2014).
2. Cespi, D., Passarini, F., Vassura, I. & Cavani, F. Butadiene from biomass, a life cycle perspective to address sustainability in the chemical industry. *Green Chem.* **18**, 1625–1638 (2016).
3. Qi, Y. *et al.* Synthesis of 1,3-butadiene and its 2-substituted monomers for synthetic rubbers. *Catalysts* **9**, (2019).
4. Dhanorkar, R. J., Mohanty, S. & Gupta, V. K. Synthesis of Functionalized Styrene Butadiene Rubber and Its Applications in SBR-Silica Composites for High Performance Tire Applications. *Ind. Eng. Chem. Res.* **60**, 4517–4535 (2021).
5. White, W. C. Butadiene production process overview. *Chem. Biol. Interact.* **166**, 10–14 (2007).
6. Zimmermann, R. W. H. ethylene (Ullmann's Encyclopedia of Industrial Chemistry). *Wiley-VCH Verlag GmbH &Co. KGaA Weinheim* (2009).
7. Duan, H., Yamada, Y. & Sato, S. Future prospect of the production of 1,3-butadiene from butanediols. *Chem. Lett.* **45**, 1036–1047 (2016).
8. Ren, T., Patel, M. & Blok, K. Olefins from conventional and heavy feedstocks: Energy use in steam cracking and alternative processes. *Energy* **31**, 425–451 (2006).
9. H.-J. Arpe. Industrial Organic Chemistry. *Wiley-VCH Verlag GmbH Co. KGaA* (2010).
10. Löser, E. G. J. . Butadiene (Ullmann's Encyclopedia of Industrial Chemisty). *Weinheim: Wiley-VCH* (2012).
11. Kang, Q., Appels, L., Tan, T. & Dewil, R. Bioethanol from Lignocellulosic Biomass: Current Findings Determine Research Priorities. *TheScientificWorld* **2014**, 298113–298153 (2014).
12. Jambo, S. A. *et al.* A review on third generation bioethanol feedstock. *Renew. Sustain. energy Rev.* **65**, 756–769 (2016).
13. Devi, A., Niazi, A., Ramteke, M. & Upadhyayula, S. Techno-economic analysis of ethanol production from lignocellulosic biomass - a comparison of fermentation, thermo catalytic, and chemocatalytic technologies. *Bioprocess Biosyst. Eng.* **44**, 1093–1107 (2021).
14. R. F. W. Goldstein, A. L. The petroleum chemical industry, E&FN. *Spon LTD, London* (1967).
15. Kirshenbaum, I. *Butadiene*. (Encyclopedia of chemical technology). New York: John Wiley & Sons, 1978).
16. Yan, W., Kouk, Q. Y., Luo, J., Liu, Y. & Borgna, A. Catalytic oxidative dehydrogenation of 1-butene to 1,3-butadiene using CO2. *Catal. Commun.* **46**, 208–212 (2014).
17. Li, S. *et al.* Dehydra-Decyclization of Tetrahydrofuran on H-ZSM5: Mechanisms, Pathways, and Transition State Entropy. *ACS Catal.* **9**, 10279–10293 (2019).
18. Abdelrahman, O. A. *et al.* Biomass-Derived Butadiene by Dehydra-Decyclization of Tetrahydrofuran. *ACS Sustain. Chem. Eng.* **5**, 3732–3736 (2017).
19. Choudhary, V., Pinar, A. B., Sandler, S. I., Vlachos, D. G. & Lobo, R. F. Xylose Isomerization to Xylulose and its Dehydration to Furfural in Aqueous Media. *ACS Catal.* **1**, 1724–1728 (2011).

20. Patent Issued for Single Step Process for Conversion of Furfural to Tetrahydrofuran. *J. Eng.* 9252 (2017).
21. Chen, S., Wojcieszak, R., Dumeignil, F., Marceau, E. & Royer, S. How Catalysts and Experimental Conditions Determine the Selective Hydroconversion of Furfural and 5-Hydroxymethylfurfural. *Chem. Rev.* **118**, 11023–11117 (2018).
22. Bucsi, I., Molnár, Á., Bartók, M. & Olah, G. A. Transformation of 1,3-, 1,4- and 1,5-diols over perfluorinated resinsulfonic acids (Nafion-H). *Tetrahedron* **51**, 3319–3326 (1995).
23. Nicola VecchiniArmando GaleottiAndrea PISANO. Process for the production of 1,3-butadiene from 1,4-butanediol via tetrahydrofuran. (2016).
24. N. d. d. m. e. c. No Title. *applicata* **2**, 693–694 (1973).
25. G. Patent DE 725532.
26. Kumar, G. *et al.* Dehydra-decyclization of 2-methyltetrahydrofuran to pentadienes on boron-containing zeolites. *Green Chem.* **22**, 4147–4416 (2020).
27. Ji, Y., Lawal, A., Nyholm, A., Gorte, R. J. & Abdelrahman, O. A. Dehydra-decyclization of tetrahydrofurans to diene monomers over metal oxides. *Catal. Sci. Technol.* **1**, 593–5912 (2020).
28. Kuznetsov, A. *et al.* On the Economics and Process Design of Renewable Butadiene from Biomass-Derived Furfural. *ACS Sustain. Chem. Eng.* **8**, 3273–3282 (2020).
29. Jain, S. K. *et al.* P-site structural diversity and evolution in a zeosil catalyst. *J. Am. Chem. Soc.* **143**, 1968–1983 (2021).
30. Kumar, G. *et al.* Dehydra-decyclization of 2-methyltetrahydrofuran to pentadienes on boron-containing zeolites. *Green Chem.* **22**, 4147–4160 (2020).
31. Kumar, G. *et al.* Acid Sites of Phosphorus-Modified Zeosils. *ACS Catal.* **11**, 9933–9948 (2021).
32. Abdelrahman, O. A. *et al.* Simple quantification of zeolite acid site density by reactive gas chromatography. *Catal. Sci. Technol.* **7**, 3831–3841 (2017).
33. Kumar, G. *et al.* Catalysis-in-a-Box: Robotic Screening of Catalytic Materials in the Time of COVID-19 and Beyond. *Matter* **3**, 805–823 (2020).
34. Beach, C. A. *et al.* Quantitative carbon detector for enhanced detection of molecules in foods, pharmaceuticals, cosmetics, flavors, and fuels. *Anal.* **141**, 1627–1632 (2016).
35. Baerlocher, C.; McCusker, L. D. of Z. S. No Title.
36. Migues, A. N., Muskat, A., Auerbach, S. M., Sherman, W. & Vaitheeswaran, S. On the Rational Design of Zeolite Clusters. *ACS Catal.* **5**, 2859–2865 (2015).
37. Svensson, M. *et al.* ONIOM: A Multilayered Integrated MO + MM Method for Geometry Optimizations and Single Point Energy Predictions. A Test for Diels−Alder Reactions and Pt(P(t-Bu)3)2 + H2 Oxidative Addition. *J. Phys. Chem.* **100**, 19357–19363 (1996).
38. Dapprich, S.; Komáromi, I.; Byun, K. S.; Morokuma, K.; Frisch, M. J. A new ONIOM implementation in Gaussian98. Part I. The calculation of energies, gradients, vibrational fre- quencies and electric field derivatives. *Theochem* **461**, 1–21 (1999).
39. Vreven,T.;Morokuma,K.;Farkas,Ö.;Schlegel,H.B.;Frisch, M. J. Geometryoptimization with QM/MM, ONIOM, and other combined methods. I. Microiterations and constraints. *J. Comp. Chem.* **24**, 760–769 (2003).
40. Vreven, T.; Byun, K. S.; Komáromi, I.; Dapprich, S.; Montgomery Jr, J. A.; Morokuma, K.; Frisch, M. J. Combining quantum mechanics methods with molecular mechanics methods

in ONIOM. *J. Chem. Theory Comput.* **2**, 815–826 (2006).
41. Zhao, Y.; Truhlar, D. G. The M06 suite of density functionals for main group thermochemistry, thermochemical kinetics, noncovalent interactions, excited states, and transition ele- ments: two new functionals and systematic testing of four M06-class functionals and 12 other func. *Theor. Chem. Acc* **I20**, 215–241 (2008).
42. Stewart, J. J. Optimization of parameters for semiempirical methods V: Modification of NDDO approximations and application to 70 elements. *J. Mol. Model* **13**, 1173–1213 (2007).
43. Naik, A. V, Joseph, K. E., Shetty, M., Ardagh, M. A. & Dauenhauer, P. J. Kinetics of 2â‘Methylfuran Acylation with Fatty Acid Anhydrides for Biorenewable Surfactants. *ACS Sustain. Chem. Eng.* **8**, 18616–18625 (2020).
44. Deng, C. *et al.* The effect of positioning cations on acidity and stability of the framework structure of Y zeolite. *Sci. Rep.* **6**, 23382 (2016).
45. Foran, G. Y., Harris, K. J., Brook, M. A., Macphail, B. & Goward, G. R. Solid State NMR Study of Boron Coordination Environments in Silicone Boronate (SiBA) Polymers. *Macromolecules* **52**, 1055–1064 (2019).
46. Khulbe, K. C., Matsuura, T., Feng, C. Y. & Ismail, A. F. Recent development on the effect of water/moisture on the performance of zeolite membrane and MMMs containing zeolite for gas separation. *RSC Adv.* **6**, 42943–42961 (2016).
47. Li, S. *et al.* Dehydra-Decyclization of Tetrahydrofuran on H-ZSM5: Mechanisms, Pathways, and Transition State Entropy. *ACS Catal.* **9**, 10279–10293 (2019).
48. Vjunov, A., Derewinski, M. A., Fulton, J. L., Camaioni, D. M. & Lercher, J. A. Impact of Zeolite Aging in Hot Liquid Water on Activity for Acid-Catalyzed Dehydration of Alcohols. *J. Am. Chem. Soc.* **137**, 10374–10382 (1900).
49. Tijink, G. A. H., Janssen, R. & Veeman, W. S. Investigation of the hydration of zeolite NaA by two-dimensional sodium-23 nutation NMR. *J. Am. Chem. Soc.* **109**, 7301–7303 (1987).
50. Yarulina, I., Kapteijn, F. & Gascon, J. The importance of heat effects in the Methanol to Hydrocarbons reaction over ZSM-5: on the role of mesoporosity on catalyst performance. *Catal. Sci. Technol.* **6**, 5320–5325 (2016).
51. Epelde, E. *et al.* Controlling coke deactivation and cracking selectivity of MFI zeolite by H3PO4 or KOH modification. *Appl. Catal. A. Gen.* **505**, 105–115 (2015).